

NAS7-1002

JPL-  
IN-84-CR

NASA 1002  
NASA CR-  
PSI-1038/TR-862

161103

P-19

MULTICOLOR PYROMETER FOR MATERIALS PROCESSING IN SPACE

PHASE II

Quarterly Report No. 4

for the period  
1 March - 31 May 1988

Michael Frish, Jonathan Frank, Henry Beerman  
Physical Sciences Inc.

August 1988

Prepared for:

NASA - JPL  
4800 Oak Grove Drive  
Pasadena, CA 91109

(NASA-CR-183189) MULTICOLOR PYROMETER FOR  
MATERIALS PROCESSING IN SPACE Quarterly  
Report No. 4, 1 Mar. - 31 May 1988  
(Physical Sciences) 19 p

CSCL 22A

N89-11057

Unclas  
G3/29 0161103

## LIST OF CONTENTS

<u>Section</u>	<u>Page</u>
1. INTRODUCTION	1
2. ANALYSIS OF FILTER COLORS	1
2.1 Background	1
2.2 Selection Algorithm	3
3. OPTICAL SYSTEM	8
4. FUTURE PLANS	15
REFERENCES	15

LIST OF ILLUSTRATIONS

<u>Figure</u>		<u>Page</u>
1.	Color selection algorithm.	5
2.	Spectral response.	6
3.	Temperature ranges covered by each of the six colors versus emissivity of the sample.	7
4.	Arrangement of multiple images on CCD detector.	8
5.	Example optical system which images a point source to three different colors with magnification 1/5.	9
6.	Exact ray trace of original optical concept.	12
7.	Multi-color optical system employing objective, field lenses, and imaging lens.	13
8.	Multi-color optical system using multiple imaging lenses.	14

## 1. INTRODUCTION

This report documents the work performed by Physical Sciences Inc., (PSI) under contract to NASA JPL, during the fourth quarter of a 2-year SBIR Phase II program. The program goals are to design, construct and program a prototype imaging pyrometer capable of measuring, as accurately as possible, the temperature distribution across the surface of a moving object suspended in space. The approach is to utilize an optical system which operates at short wavelengths compared to the peak of the blackbody spectrum for the temperature range of interest, thus minimizing errors associated with a lack of knowledge about the heated sample's emissivity. To cover a broad range of temperatures, several wavelengths are required. The preferred wavelength decreases as the temperature increases.

Previously,<sup>1</sup> we performed a survey of available imaging technologies and selected the Sierra Scientific Model 4032 CCD camera as the sensor to be used by our pyrometer. An analysis of the system's temperature measurement capability based on this camera's responsivity was performed and found to be satisfactory. Subsequently, the camera was purchased and coupled to a Compaq 286 computer through a Data Translation Model 2851 frame-grabber. A unique interface between camera and computer was designed and assembled which allows the computer to electronically control the exposure time of each frame.<sup>2</sup> The overall system noise was measured as a function of integration time for use in optimizing the pyrometer's operation.<sup>3</sup>

We had also reported previously a conceptual design of the optical system which will image of the sample onto the CCD detector.<sup>2</sup> The system maximizes use of the spatial resolution available on the detector and projects images at all of the desired wavelengths simultaneously. As a result, the multi-color pyrometer will require no moving parts and will have the capability to calculate temperatures by ratio pyrometry when appropriate, as well as by use of each color individually.

In this report we discuss the details of the evolving optical design and our progress towards construction of a working breadboard model. In addition, details of the algorithm developed for selecting the optimum colors to be used by the pyrometer are reported. Though final selection of the colors will have to await a final design of the optical system, results using a preliminary optical design are presented.

## 2. ANALYSIS OF FILTER COLORS

### 2.1 Background

As described in our third quarterly report,<sup>3</sup> the sequence of events yielding one temperature measurement with the pyrometer will be as follows: The radiation emitted by the heated object is passed through a system of beam

splitters and lenses which form six separate images on the camera's CCD detector array. Before reaching the detector the light of each image passes through one of six narrow bandwidth interference filters. These photons generate photoelectrons at the individual CCD photosensitive sites. Electrical charge is collected for a period of time determined by a computer-controlled interface described in our second quarterly report. At the end of this integration period, the accumulated charge is transferred out of the CCD array, passed through a transimpedance amplifier which has a user selectable gain, and converted to an output voltage. The charges from the pixels are read out sequentially, resulting in a temporally varying voltage signal, the voltage at any given time being directly proportional to the charge accumulated at the corresponding pixel site during the integration time. This output voltage is then coupled into the frame grabber and digitized by the 8-bit a/d converter. During digitization, each pixel is assigned an integer value, or a/d level, between 0 and 255 proportional to its voltage. The results of the digitization are stored in computer memory and can be transferred to disk if desired. The values can then be recalled from memory or disk and converted to temperatures.

The procedure for calculating temperature has been thoroughly discussed in previous reports.<sup>4</sup> However, because of its importance in determining the precision of the temperature measurement and the selection of wavelengths at which to operate the pyrometer, we briefly discuss it again here. The basic equation describing the operation of any temperature-sensitive radiometer is

$$V = GN = \frac{2Gc\varepsilon_{\lambda}\eta_{\lambda}\tau_{\lambda}A_p\Omega\Delta\lambda}{M^2\lambda^4[\exp(hc/\lambda kT) - 1]} \quad (1)$$

where  $V$  is the output voltage of the radiometer's electro-optic system, determined by the transfer constant,  $G$ , and the number of photoelectrons,  $N$ , generated at one detector pixel of area  $A_p$ , onto which a source area  $A_p/M^2$  is imaged.  $M$  is the magnification of the optical system,  $\Omega$  is the solid angle subtended by the optics,  $\lambda$  is the central wavelength of a bandpass  $\Delta\lambda$  over which the samples' radiance is observed,  $\varepsilon_{\lambda}$  is the emissivity of the sample at that wavelength,  $\eta_{\lambda}$  the quantum efficiency of the photodetector,  $\tau_{\lambda}$  the exposure time, and  $t_{\lambda}$  is the overall transmittance of the optical system. The constants  $h, c,$  and  $k$  are Planck's constant, the speed of light, and Boltzmann's constant respectively. The goal of the pyrometer design is to select components which yield a detectable number of photoelectrons during the desired exposure time, while maximizing the accuracy and precision of the temperature measurement.

The accuracy of the complete system is determined by the accuracy with which the parameters in Eq. (1) can be evaluated, either by calibration or calculation. As was discussed in our Phase I report,<sup>4</sup> the largest uncertainty is the emissivity of the heated sample,  $\varepsilon_{\lambda}$ . For most materials of interest, the emissivity during processing will generally be poorly known. Thus, to calculate the temperature, an educated guess of the emissivity is usually used

in Eq. (1). When wavelengths have been selected such that  $\lambda T \ll hc/k = 1.44$  cm-K, the temperature error resulting from an error in the assumed emissivity is given by

$$\frac{\Delta T}{T} = \frac{k\lambda T}{hc} \frac{\Delta \epsilon}{\epsilon} \quad (2)$$

Minimizing the resultant temperature error, or maximizing the pyrometer's accuracy, therefore requires operating the pyrometer at as short a wavelength as possible. At first glance, it would appear that the optimum wavelength is that which, at the minimum desired operating temperature, yields a value of  $N$  which is equal to the system noise (assuming that the system noise is large compared to the photon shot noise). However, this procedure can lead to creation of a pyrometer in which the precision of the temperature measurement is poor.

The precision of the temperature measured by a pyrometer is determined by the data acquisition device which measures the output of the electro-optic transducers, which in our system is the video frame grabber. The frame grabber has 8-bit precision, meaning that a 1-bit signal change, which is the minimum resolvable change in signal, is  $1/(2^8-1) = 1/255$  of the signal at saturation. If each color in the pyrometer is configured so that at the maximum temperature for which that color is sensitive its output signal equals the maximum accepted by the frame grabber, then the worst temperature precision is equal to the temperature change that causes a 1-bit signal change at the lowest temperature within the color's operating range.

## 2.2 Selection Algorithm

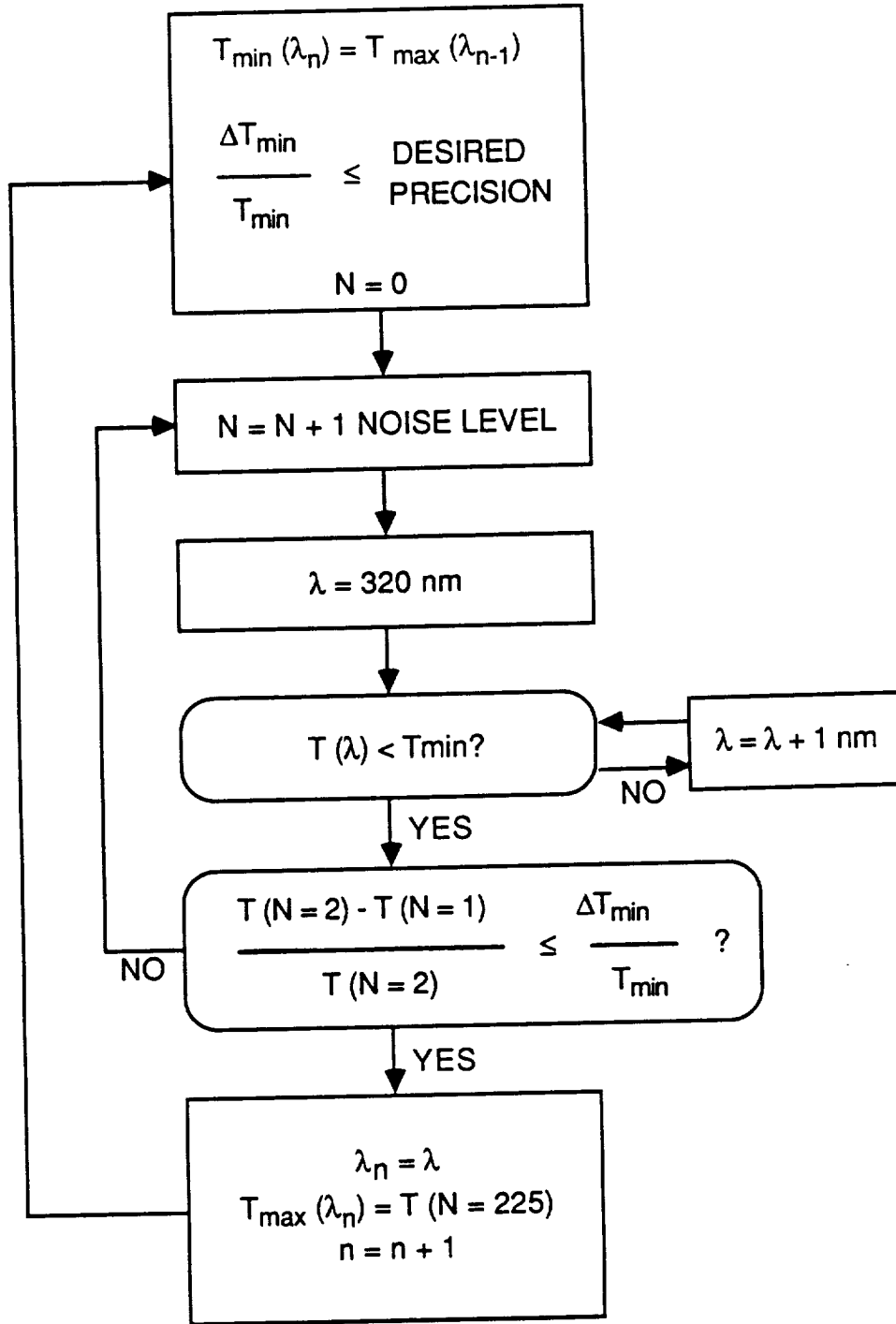
The first step in determining the best set of colors is to choose the wavelength-independent parameters which are included in Eq. (1), namely the solid angle, integration time, pixel size, and system magnification. Since our pyrometer will have no moving or interchangeable parts, these parameters are fixed by the hardware selected for its construction (except for integration time, which is variable over about two orders of magnitude.) Next, the wavelength which provides the minimum detectable temperature is found. The minimum detectable temperature at a particular wavelength is that which generates an average number of photoelectrons equal to the detector's rms noise. (As discussed in our third quarterly report,<sup>3</sup> the noise level is actually a function of the pixel value. At zero average signal there are about 300 electrons rms of noise, while near saturation there are about 900 electrons. In these calculations, we have assumed a noise level of 675 electrons. Note that by setting the camera gain so that this noise level is equal to the first digitizer step, the minimum detectable temperature is that which increases the pixel output by one a/d level.) By calculating the minimum detectable temperature as a function of wavelength, including in the calculation the decrease of quantum efficiency as the wavelength increases above 600 nm, the wavelength of the absolute minimum measurable temperature is found. This determines the lower limit of the pyrometer's sensitivity given

the previously selected fixed parameters. This wavelength is selected as the longest of the six. The maximum temperature observable at this wavelength is determined by calculating the number of photoelectrons which produce a signal of 255 a/d levels.

Though this wavelength enables measurement of the lowest temperature possible for the selected hardware, it does not necessarily provide the high precision needed if temperature gradients are to be accurately determined. The wavelengths of all remaining colors are calculated on the basis of achieving a predetermined precision. Because the number of photoelectrons generated at a specific wavelength increases much more rapidly than linear with increasing temperature, the precision of the measurement also increases with temperature. That is, at higher temperatures a smaller change in temperature is required to produce an incremental step in the a/d level of the digitizer than at lower temperatures. Thus, if a predetermined precision is desired, then the minimum temperature at which this precision can be achieved may be higher than the absolute minimum temperature and may occur at some a/d level greater than 1. Each additional color therefore has specified both a wavelength and a minimum a/d level for optimum operation. Of course, if the a/d level is greater than two, lower temperatures can be measured at the selected wavelength, but with reduced precision.

Each new wavelength is found using the algorithm shown in the flow chart of Figure 1. The minimum temperature measurable with the desired precision at each wavelength is selected to be slightly lower than maximum temperature measurable at the next longest wavelength. Starting with a number of photoelectrons equal to the noise level, the temperature is calculated as a function of wavelength, and the wavelength found where the temperature is equal to the desired minimum. Then the precision at that temperature and wavelength is calculated. If the precision is inadequate, i.e.,  $\Delta T/T$  is too large, then the number of photons, or equivalently the minimum usable a/d level, is increased by one additional noise level and the procedure repeated until a wavelength and an a/d level at which the desired minimum temperature can be measured with the desired precision are found. This procedure is repeated until all six wavelengths are determined.

Since the color selection algorithm requires knowledge of the optical throughput it is obviously necessary that a working optical system be fully designed prior to final selection of the colors. Nevertheless, the algorithm has been exercised to make a preliminary specification of the wavelengths required to span the range of temperatures between the minimum detectable and 2500 K with the best precision. For this calculation, the sample's emissivity was assumed to be 0.5. The transmission of the optics was estimated on the basis of using two glass lenses, and the quantum efficiency of the CCD detector was interpolated from the spectral response graph provided by Sierra Scientific for the Amperex 1031 CCD array, shown in Figure 2. The standard video integration time of 16.67 ms was assumed, and the optical collection efficiency was chosen as F/10. It was found that a minimum temperature of about 900 K was measurable, and that temperatures between 955 K and 2680 K could be measured with 0.45% precision. The selected wavelengths, their



A-8863

Figure 1. Color selection algorithm.

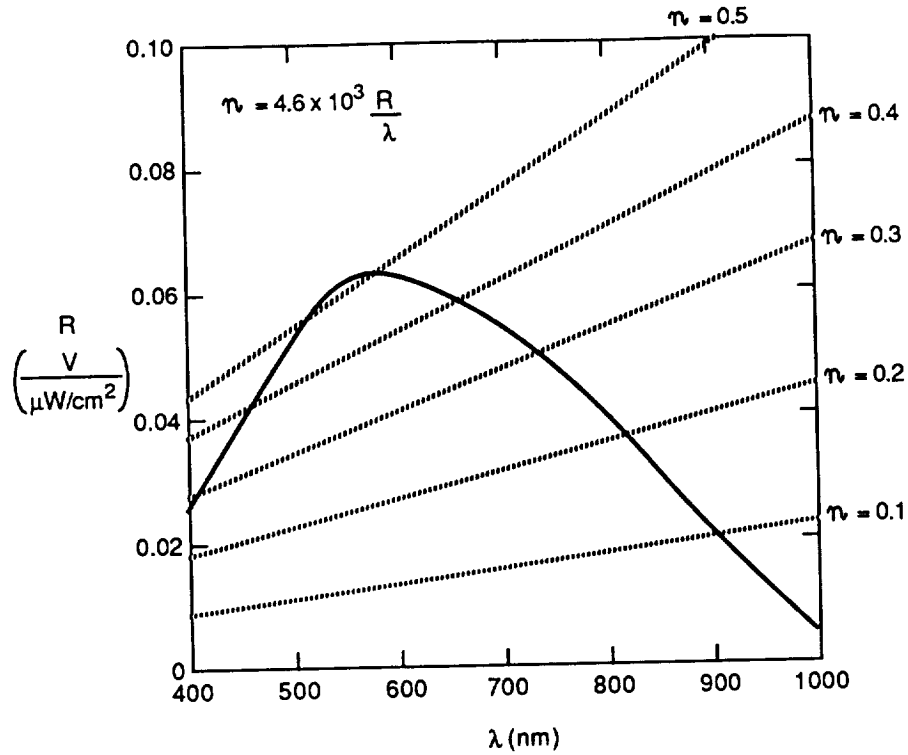
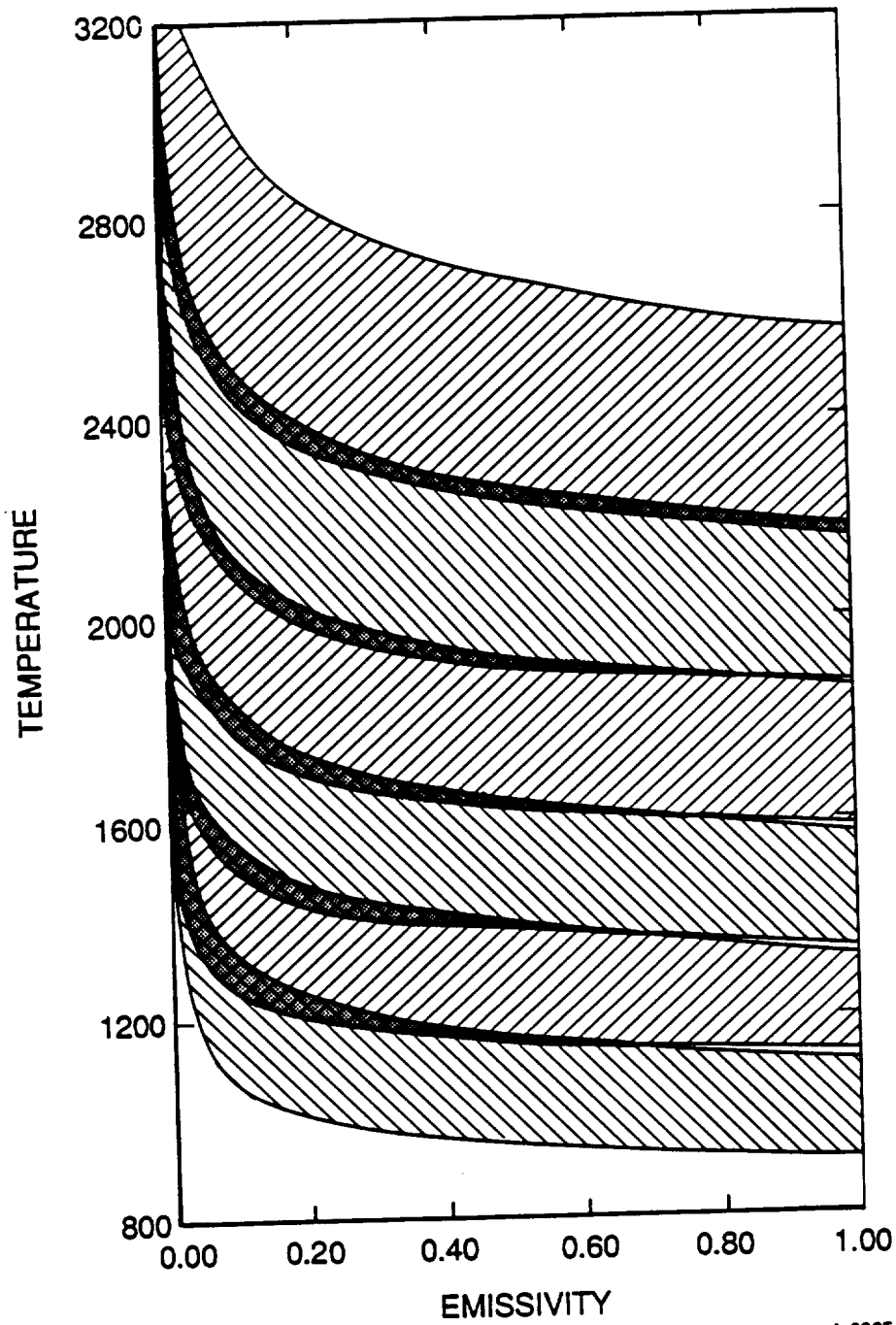


Figure 2. Spectral response.

temperature ranges, and the a/d level at the lowest temperature having the desired precision are as follows:

Wavelength (nm)	High Temp. (K)	Low Temp. @ 0.45% precision	Minimum a/d level
919	1161	954	9
631	1383	1160	6
511	1637	1382	6
415	1920	1634	6
359	2261	1919	6
326	2679	2248	6

Figure 3 graphically displays the range of temperatures measurable at each of these wavelengths as a function of the sample's emissivity. In the shaded regions the upper range of one filter overlaps with the lower range of the filter of next shorter wavelength. Though it appears that there is a slight gap in temperature measurement capability at low temperatures and high emissivities, the gap can be closed by reducing the integration time slightly for high emissivity materials. Furthermore, the lower temperature limit can be



A-8865

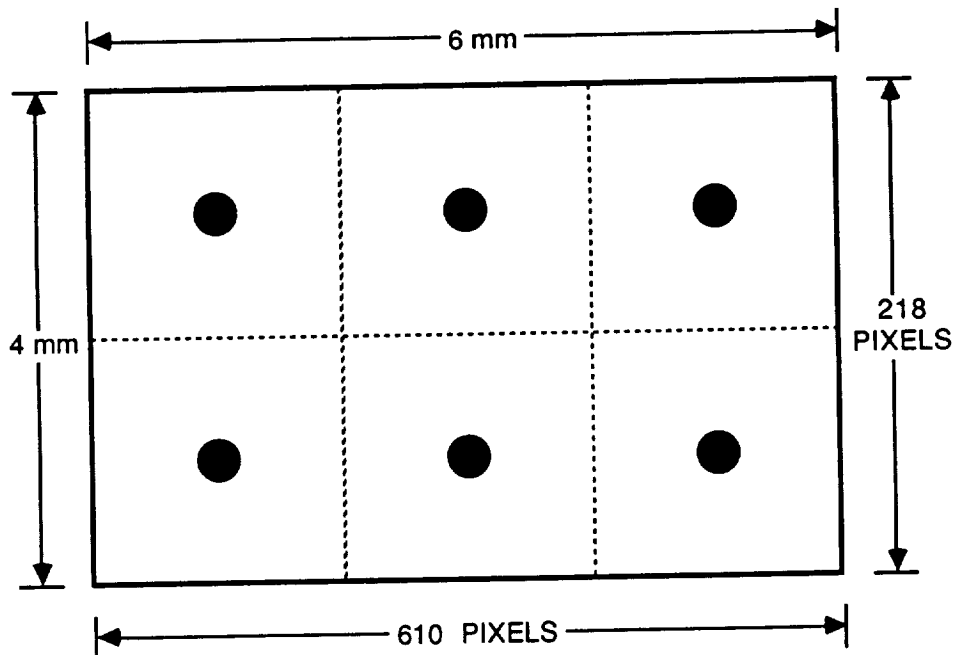
Figure 3. Temperature ranges covered by each of the six colors versus emissivity of the sample.

reduced by increasing the integration time. Thus, through the use of the computer controlled variable integration time camera and these filters, wide flexibility in the the operation of the system is possible.

### 3. OPTICAL SYSTEM

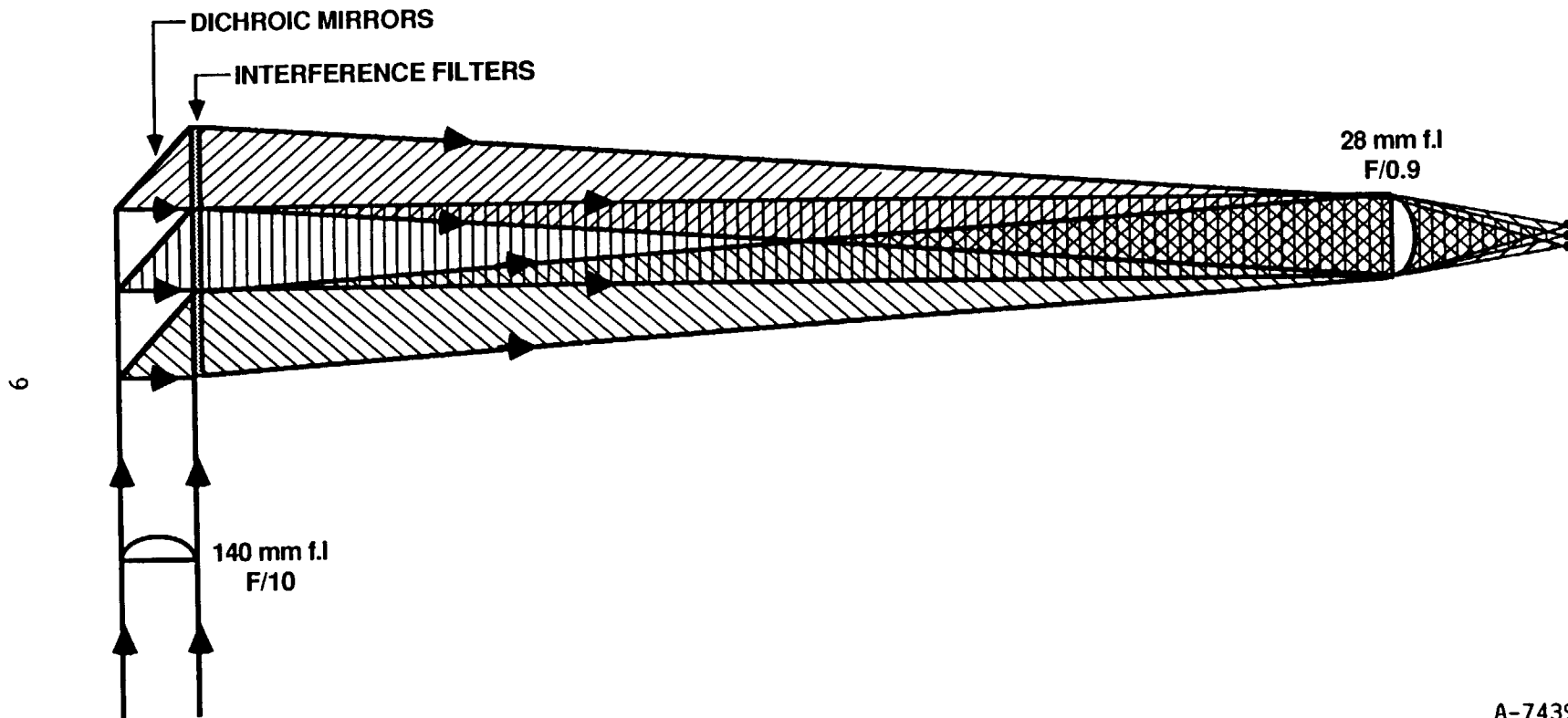
In our second quarterly report,<sup>2</sup> we presented a conceptual optical system which projects six different-color images onto the CCD array simultaneously. Figure 4 is a view of the detector surface, which is 6 mm wide and 4 mm high. We have shown it broken into six regions, each 2 mm x 2 mm onto which six images of the sample are projected. Assuming a magnification of 1/5, each sector observes an area of 1 cm x 1 cm around the sample, the maximum area over which the sample is expected to move during processing.

Figure 5 is an illustration of the original concept for a color separator and imaging system for providing these six different-colored views. For convenience, only three colors are shown. In this system, radiation emitted by the sample is collected by an objective lens. The heated sample is located nearly within the focal plane of the lens, thereby projecting a nearly-collimated beam of light into the color separator. This beam is separated into color ranges by a series of dichroic mirrors. The first mirror ideally reflects all radiation at wavelengths greater than  $\lambda_1$  while transmitting all shorter wavelengths. The second mirror similarly reflects all radiation at



A-7438

Figure 4. Arrangement of multiple images on CCD detector.



A-7439

Figure 5. Example optical system which images a point source to three different colors with magnification 1/5.

wavelengths longer than  $\lambda_2$  (of which there is none longer than  $\lambda_1$ ) and transmits the rest, which is reflected by the third mirror. The three reflected beams are transmitted through interference filters, which select the desired narrow bands of wavelengths from the relatively broad bands reflected by the beamsplitters. The three reflections are then superimposed upon each other at the surface of an imaging lens, each forming an image at the focal plane. Since the three beams arrive at the lens from different angles, the images are laterally separated from each other by a distance equal to the focal length multiplied by the tangent of the relative angular separation. The overall system magnification is determined by the ratio of the focal lengths of the two lenses.

This concept can be extended to provide six separate images by adding a fourth dichroic beamsplitter ahead of the three shown, which reflects a band of wavelengths upwards to a second row of beamsplitters positioned above the layer shown. The reflections from this second layer would also be projected onto the imaging lens, which would now be centered on the plane separating the two beamsplitter layers, resulting in two layers of reflections. By selecting the desired number of layers and number of beamsplitters in each layer, any number of different colors can in principle be accommodated. However, the maximum number of colors is ultimately fixed by the sizes of the components and the overall system magnification (which determines the number of views which can be projected on the detector simultaneously from a fixed-size object), and conversely. Furthermore, to avoid the need for pixel-by-pixel calibration of the system, and subsequent time consuming pixel-by-pixel correction of the image, it is desirable that the optics be as free as possible of aberrations and vignettes. The goal of the optical design is to select components which maximize the amount of light which is collected and properly imaged onto the detector at each of the six colors. Designing a system which has both high throughput and little aberration has proven to be more difficult than expected. A discussion of the problems encountered follows.

Our first effort was to perform an engineering feasibility study of the conceptual system shown in Figure 5. In this design, the overall path length of the reflected beams is fixed by their angular separation and the diameter of the objective lens. It had been assumed initially that the objective lens would have a focal length of 140 mm and a diameter of 14 mm, i.e. a speed of F/10. The objective lens was to have been positioned one focal length from the object plane, where the desired field of view is 10 mm in diameter, so that each collimated beam would have a full-angle divergence of  $\tan^{-1}(10/140) = 4$  deg. Assuming that the dichroic mirrors were ideally spaced, that is precisely one beam diameter apart, then at the imaging lens the superimposed collimated beams would have diameters of 32 mm. To focus these beams with a magnification of 1/5, the imaging lens would need a focal length of 28 mm, and therefore a speed of F/0.9.

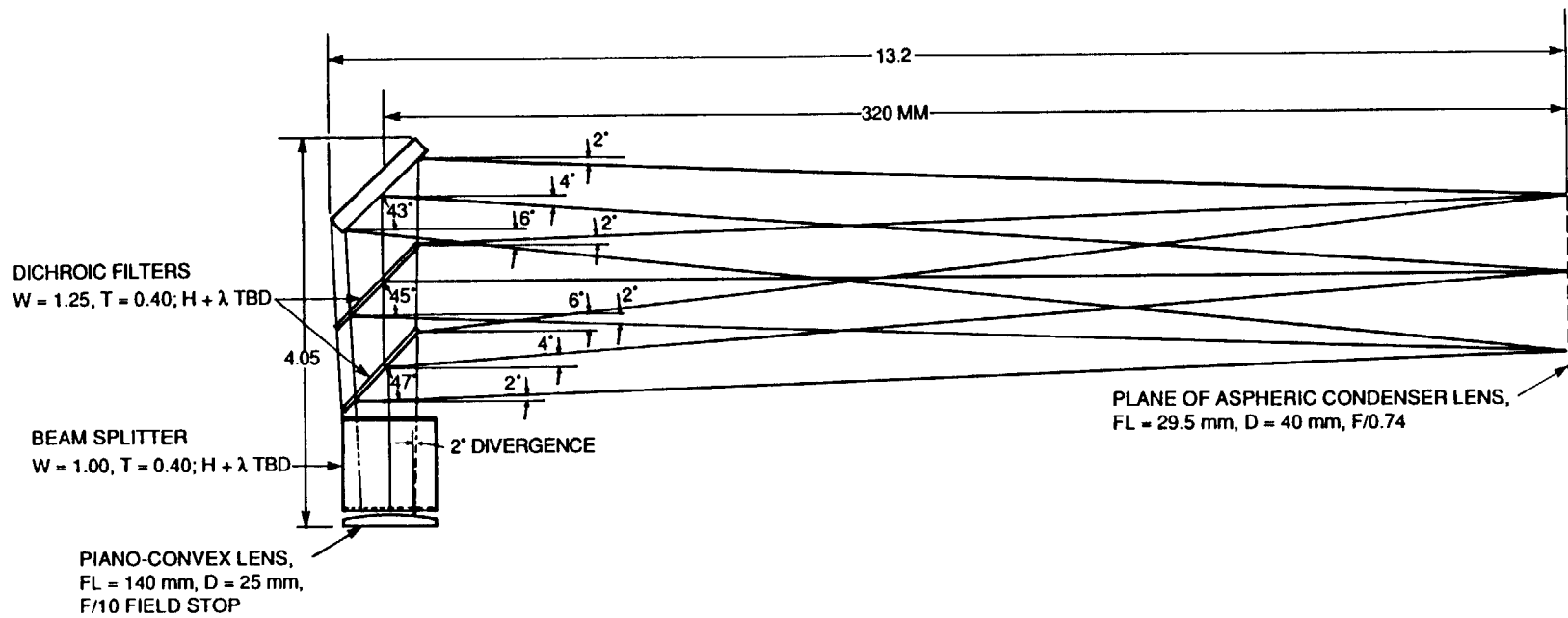
During the engineering evaluation of this design it was found, not surprisingly, that the dichroic beamsplitters could not readily be separated by only one beam diameter. At least one extra millimeter was required simply

to allow for the thickness of the mirrors. Due to the shallow angles at which the multiple beams converge on the imaging lens, this slight increase in the separation of the beamsplitters was found to materially increase the overall distance required to overlap the beams, and thus also increased the beam diameter at the imaging lens. A realistic ray tracing diagram is presented in Figure 6, where it is seen that the distance to the imaging lens must be about 320 mm. The beam diameter at that lens is then about 40 mm, requiring a lens speed of F/0.70. Unfortunately, lenses of this short focal length and speed suffer from severe aberrations. We tested an aspheric condenser lens, which is the most aberration free high-speed lens available, and found its performance to be completely unacceptable for this application. As a result, we were forced to abandon this simple optical design and resort to the next level of complexity.

The next design considered and experimentally attempted is illustrated in Figure 7. It employed individual field lenses for each collimated beam to decrease the diameter of the beams when they reach the focusing lens, thereby allowing the use of slower speed optics such as off-the-shelf camera lenses. However, because the distance from the focusing lens to the detector surface was reduced by the addition of the field lenses, the relative angle between the beams needed to be increased compared to the previous design in order to maintain adequate separation of the images while maintaining the speed and magnification of the system. To minimize this angle, it was preferable to select field lenses having diameters as small as possible without introducing vignetting. This required minimizing the divergence of the collimated beams, which in turn was achieved by increasing the distance between the source and the objective and correspondingly increasing the objective's diameter and thus the overall size of the system. A design which appeared to be adequate used a 350 mm focal length, 40 mm diameter objective (with the source located 400 mm away), field lenses having focal lengths of 153 mm and 42 mm diameter, and an 8 mm focal length, F/1.3 imaging lens. This design allowed convergence angles between the beams of 18 deg.

To test this design, we purchased for use as the imaging lens a high quality wide-angle video lens from D.O. Industries which we expected would be sufficiently corrected for aberrations at these relatively large incident angles to suit our needs. Unfortunately, we were disappointed. At 18 degrees angle of incidence, severe vignetting was experienced, apparently because the limiting stop within the lens was located some distance in front of the first principle plane. Furthermore, even at zero angle of incidence, either vignetting or aberrations created excessive non-uniformities in the intensity of the image of a uniform intensity object. (A blackbody, with a 1 cm aperture, operated at 1273 K, was used for this test.) Although it may be possible to alleviate these difficulties by choosing alternate imaging lenses, it is unfortunately nearly impossible to predict the system characteristics without experimentally testing them due to the lack of data provided with commercial video lenses. We felt that this was a fruitless path to follow, and thus abandoned this second approach.

12



A-8866

Figure 6. Exact ray trace of original optical concept.

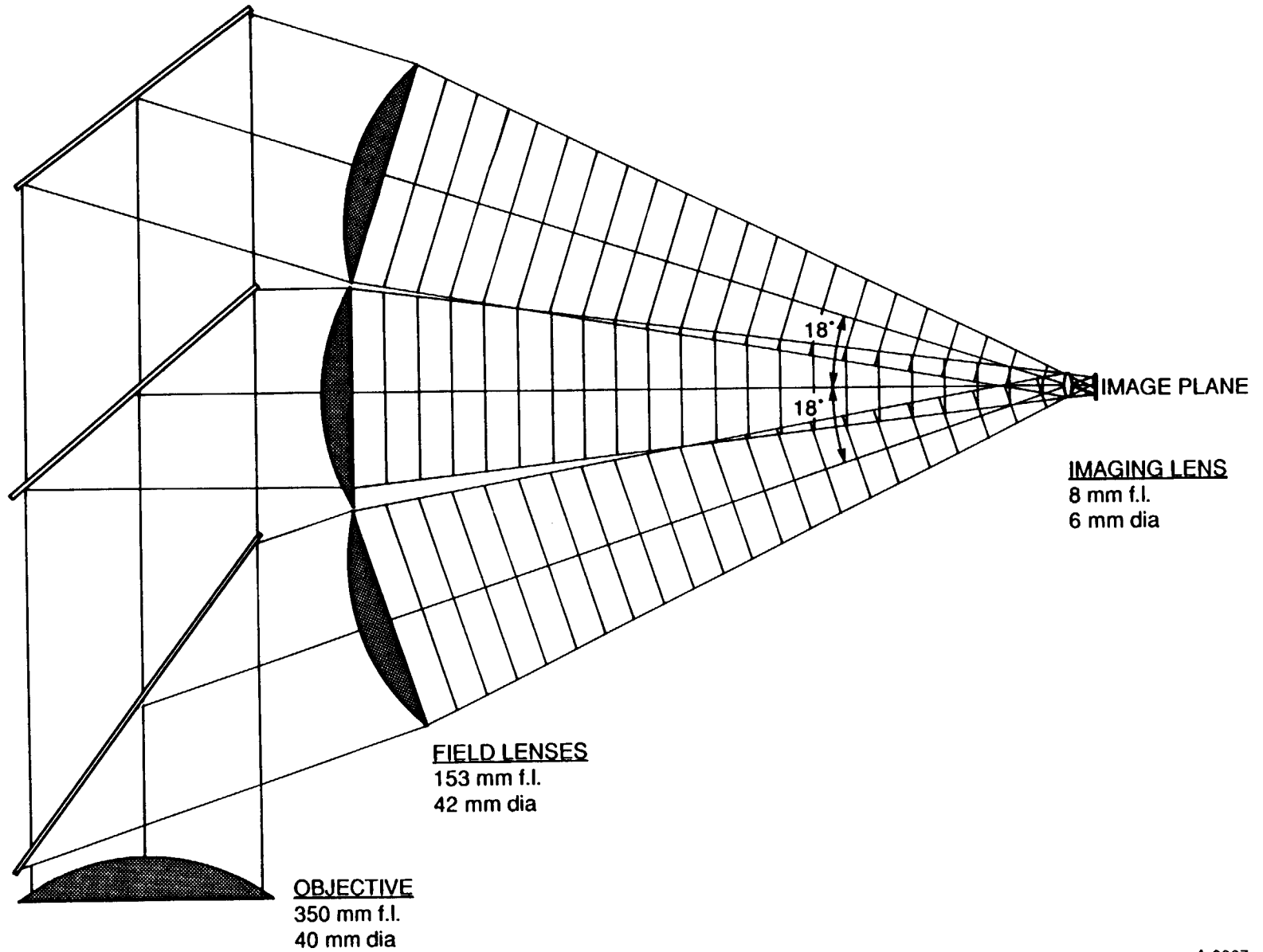


Figure 7. Multi-color optical system employing objective, field lenses, and imaging lens.

The approach now under consideration is to eliminate the imaging lens, and image with the field lenses alone, as illustrated in Figure 8. In this case, to achieve an overall system magnification of 1/5, each field lens must have a focal length 1/5 that of the objective and a speed slightly faster than F/2 without severe aberration. Since the angles of incidence on the field lenses are now nearly zero for all of the colors, this approach does not require the use of sophisticated camera lenses which are supposedly corrected for off-axis aberrations. Simple two-element achromats which are well corrected for spherical aberration should be adequate. The most severe problem with this approach is that the separated beams will be incident on the CCD detector at an angle of 20-30 degrees, thereby introducing a slight distortion of the image. A circle will be spread out into an ellipse with a major axis about 6-15 percent longer than the minor axis. However, this should not present difficulties in temperature measurement, since the reduced intensity caused by the spreading of the image can be easily compensated by a corresponding change in the calibration constant for the wavelength of interest.

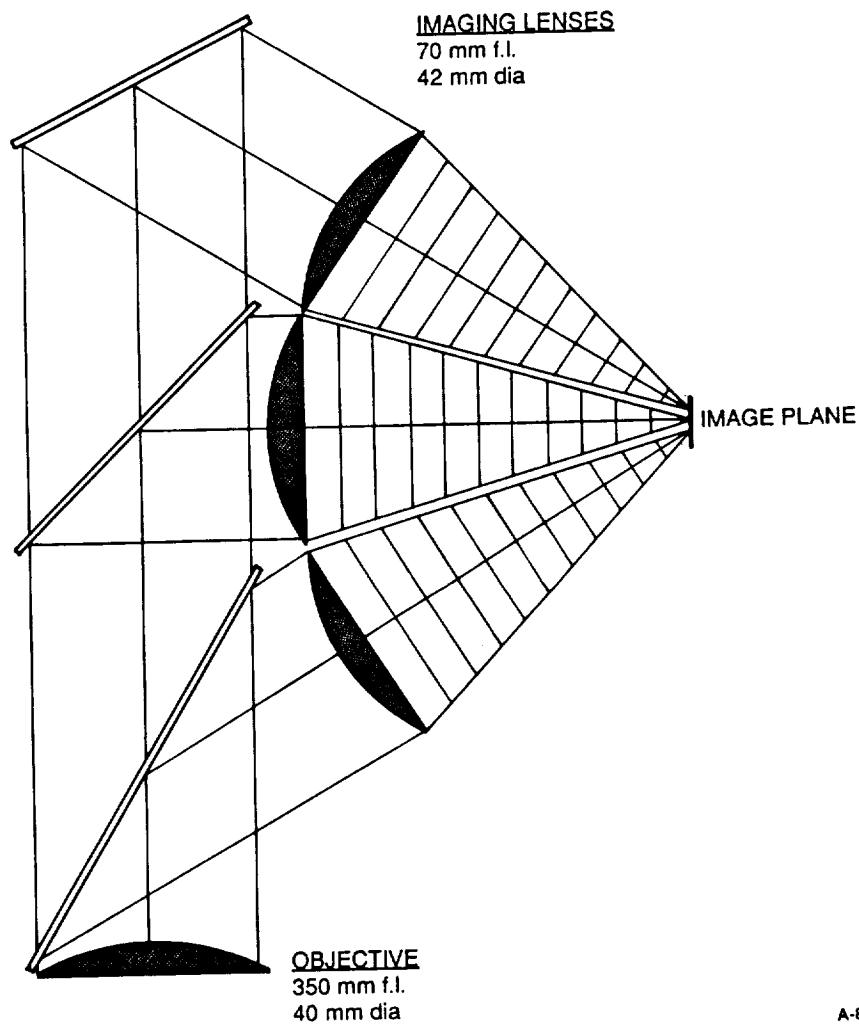


Figure 8. Multi-color optical system using multiple imaging lenses.

We have tested this technique using a 350 mm focal length, achromatic lens as the objective, and 70 mm focal length plano-convex field lenses. We found that aberration from the imaging lens was still excessive. However, when the aberration was reduced by stopping down the objective, a very uniform image with the correct magnification was obtained. Furthermore, the image uniformity was maintained even at a 30 degree angle of incidence. Thus, if the aberration is eliminated, this approach appears to offer success. We are now awaiting the delivery of a set of 78 mm achromatic lenses to use as field lenses with which we hope to eliminate the aberrations.

#### 4. FUTURE PLANS

During the next two quarters, we plan to complete the breadboard optical assembly, select the appropriate set of colors, and begin final construction of a working pyrometer. Programming the computer to select the appropriate color among the six available will proceed concurrently. We also plan to begin studying techniques for using the pyrometer to measure temperatures of objects which become transparent upon heating.

#### REFERENCES

1. Allen, M. and Frish, M., "Multicolor Pyrometer for Materials Processing in Space - Phase II. Quarterly Report No. 1", TR-731, Physical Sciences Inc., Andover MA. (November 1987).
2. Frish, M. and Frank, J., "Multicolor Pyrometer for Materials Processing in Space - Phase II. Quarterly Report No. 2", TR-764, Physical Sciences Inc., Andover MA. (February 1988).
3. Frish, M. and Frank, J., "Multicolor Pyrometer for Materials Processing in Space - Phase II. Quarterly Report No. 3", TR-796, Physical Sciences Inc., Andover MA. (May 1988).
4. Frish, M., Spencer, M., Wolk, N., Werner, J., and Miranda, H., "Multicolor Pyrometer for Materials Processing in Space - Phase I Final Report", TR-590, Physical Sciences Inc., Andover MA. (July 1986).

